Biophysical Journal, Volume *121*

Supplemental information

Extracellular and intracellular components of the impedance of neural tissue

Claude Bedard, Charlotte Piette, Laurent Venance, and Alain Destexhe

Extracellular and intracellular components of the impedance of neural tissue

Claude Bedard[1], Charlotte Piette[2], Laurent Venance[2] and Alain Destexhe[1]

1: Paris-Saclay University, CNRS, Institute of Neuroscience (NeuroPSI), Gif sur Yvette, France
2: Center for Interdisciplinary Research in Biology (CIRB), Collège de France, CNRS, INSERM, PSL University, Paris, France

January 24, 2022

Condensed title: Neural tissue impedance

Keywords: Local field potential, Extracellular space, Ionic diffusion

Supplemental Information

Appendices

Physical meaning of the method used to measure the impedance

In our experimental situation, we inject a current which is time-dependent, in a linear medium. In such conditions, the potential (relative to ground) is given by the general relation:

$$V(t,\vec{x}_{intra}) - V(t,\vec{x}_{extra}) = [V_{rest}(\vec{x}_{intra}) - V_{rest}(\vec{x}_{extra})] + \int_{-\infty}^{+\infty} Z(t-t')I_s^g(t')\ dt' \ ,$$

where $V_{rest}(\vec{x})$ is the resting potential at position $\vec{x}$ (at rest, $I_s^g(t) = 0$). It follows that, in Fourier frequency space, the potential between intracellular and extracellular electrodes is given by:

$$[V(\omega,\vec{x}_{intra}) - V_{rest}(\vec{x}_{intra})\delta(\omega)] - [V(\omega,\vec{x}_{extra}) - V_{rest}(\vec{x}_{extra})\delta(\omega)] = Z(\omega)I_s^g(\omega) \ ,$$

where $\delta(\omega)$ is the Dirac distribution. Thus, we can write:

$$V(\omega,\vec{x}_{intra}) - V(\omega,\vec{x}_{extra}) = Z(\omega)I_s^g(\omega)$$

when $\omega \neq 0$. For $\omega \neq 0$ we have $\delta(\omega) = 0$ and thus $V(\omega,\vec{x}) = V(\omega,\vec{x}) - V_{rest}(\omega,\vec{x})$ because $V_{rest}(\omega,\vec{x}) = V_{rest}(\vec{x})\delta(\omega)$. It follows that, if $\omega \neq 0$, then the potential measured as a function of frequency $V(\omega,\vec{x})$ is equal to its variation relative to that of the cell at rest. Thus, for current amplitudes that are not too strong (to remain in the linear regime), $V(\omega,\vec{x})$ has a very smooth variation in space, despite the fact that the potential at rest may show very abrupt spatial variations near the membrane. In the manuscript, we have designed by equipotential surface any surface for which $V(\omega,\vec{x}) = constant$ when $\omega = constant \neq 0$.

A Equivalent impedance between the extracellular electrode and the ground

In this appendix, we give the explicit expressions to calculate the impedance between the extracellular electrode and the ground in the different experimental conditions considered.

When measuring the equivalent impedance, we have $(Z_a \parallel Z_s \parallel Z_d) \oplus Z_g$, where Z_g is the impedance between the ground and the first isopotential surface that surrounds the neuron. Z_a is the impedance of the extracellular medium in contact

with the isopotential surface S_2, Z_s is the impedance of the current flowing through the soma membrane in contact with surface S_2, and Z_d is the input impedance of the dendritic tree relative to a reference outside the neuron (Fig. 6).

Thus, we obtain

$$\frac{V_i}{I_s^g} = Z_{eq} = \frac{Z_a Z_s Z_d}{Z_a Z_s + Z_s Z_d + Z_d Z_a} + Z_g \tag{A.1}$$

where $I_s^g = I_a^g + I_s^g + I_d^g$. I_s^g is the generalized current produced by the current source, because in our experiments, the generalized current conservation applies. Note that this does not account for charges created by chemical reactions [36]. We have

$$\begin{cases} Z_a &= R_a \\ Z_s &= Z_m + Z_e^{(m)} = \frac{r_m}{A_s(1+i\omega\tau_m)} + \frac{z_e^{(m)}}{A_s} \\ Z_d &= \frac{Z_m + Z_e^{(m)}}{Z_m} \frac{z_i}{\kappa_\lambda} \, coth(\kappa_\lambda l_d) \end{cases} \tag{A.2}$$

Here, we calculated Z_d as follows. The part of the current source that flows through the dendrite before eventually going to the ground (I_d^g) is such that we obtain $Z_{in}^d = \frac{V_m}{I_d^g} = \frac{z_i}{\kappa_\lambda} coth(\kappa_\lambda l_d)$ where V_m is the somatic membrane potential at the basis of the dendrite [22]. In addition, applying the generalized current conservation gives the following equality:

$$\frac{V_i^{S_2}}{Z_m + Z_e^{(m)}} = \frac{V_m}{Z_m} \tag{A.3}$$

where the potential $V_i^{S_2}$ is taken at the isopotential surface S_2. Thus, we have approximately:

$$Z_d = \frac{V_i}{I_d^g} = \frac{Z_m + Z_e^{(m)}}{Z_m} Z_{in}^d = \frac{Z_s}{Z_m} Z_{in}^d \tag{A.4}$$

B RC circuit in series with a resistance

In this appendix, we compare the RC model ($(R \parallel C)$) with the RC model in series with a resistance ($(R \parallel C) \oplus R*$). One can see from Fig. B.1 that the impedances of these two models are similar for small frequencies. However, they differ at high frequencies relative to the cut-off frequency of the RC circuit. It is important to also consider that the phase of the RC model tends to -90^o when frequency tends to ∞, but it tends to 0^o for the RC model in series with a resistance.

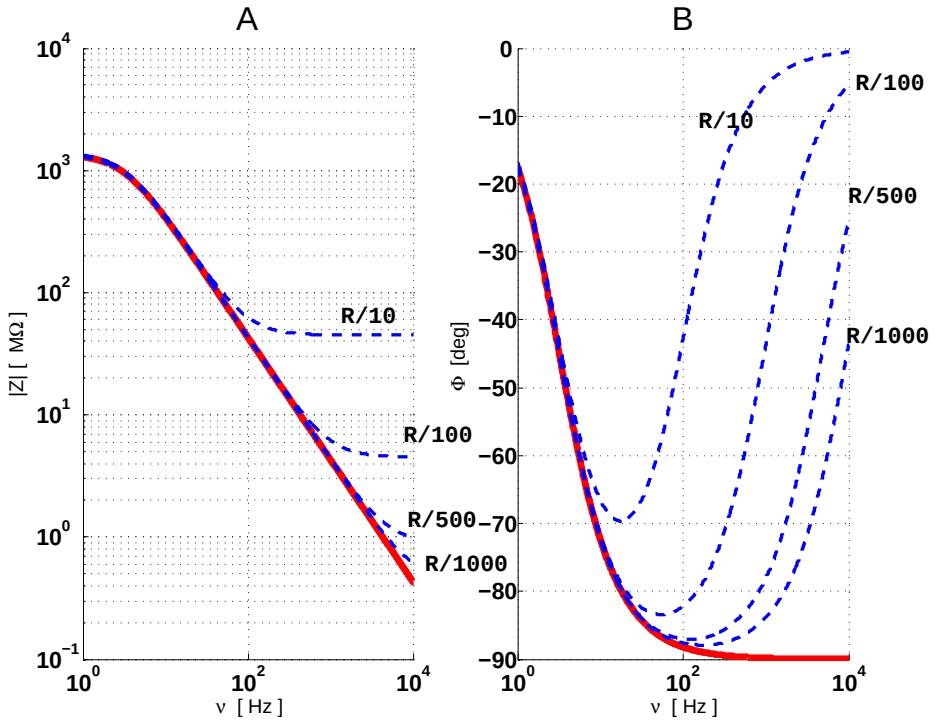

Figure B.1: Comparison betwen the impedances of the model RC ∥ (red) and of the model RC ∥ in series with a resistance (blue). The modulus (**A**) and phase (**B**) are shown as a function of frequency.

C Diffusive impedance in heterogeneous media for a spherical source

In this appendix, we present the theoretical expression of the macroscopic impedance in the case of a diffusive model [20].

In a previous publication [20], we have shown that the macroscopic diffusive impedance (also called Warburg impedance) is derived by a linear approximation of the ratio $\frac{V}{I^g}$, where V is the potential difference between the two measurement points. This derivation took into account Boltzmann distribution and Ohm's law.

The energy given to the charges divides into two parts: one dissipative part (calorific energy) and the part corresponding to the spatial arrangement and distribution of charges as a function of time. The first part is related to Ohm's law, and the second part to Nernst law.
The presence of a current source in a homogeneous medium breaks its homogeneity. Indeed, the charge distribution around the source cannot be considered constant. The application of Boltzmann's law in the quasistatic regime (in the sense of classical statistical thermodynamics), in the linear approximation, gives an impedance for a spherical current source of the form:

$$Z_\omega = \frac{CkT}{(\frac{1}{R} + \sqrt{-i\frac{\omega}{<\beta>|_m}})} \tag{C.1}$$

where C is a constant which depends on the electric conductivity of the medium in the absence of the source, R is the radius of the spherical source (which gives a curvature of $1/R^2$), T is the absolute temperature in Kelvins, $<\beta>|_m$ is equivalent to an "effective" diffusion coefficient which is negative, and $k = 1.38 \times 10^{-23}\ J/^oK$ is the Boltzmann constant (for more details, see [20]). This model is called "diffusive model", and is used here for the particular case of a spherical source.
By setting

$$A_w = CRT \tag{C.2}$$

and

$$\omega_{wT} = -\frac{<\beta>|_m}{R^2} \tag{C.3}$$

we can write expression C.1 as above:

$$Z_w = \frac{A_w}{1 + \sqrt{i\frac{\omega}{\omega_{wT}}}} \tag{C.4}$$

At constant temperature, the measurement of the impedance allows one to determine the values of A_w and $\omega_{wT} = 2\pi\nu_{wT}$. The parameters A_w and ω_{wT} are real.
However, we assumed

$$Z_w = \frac{A_w}{1 + \sqrt{i\frac{\omega}{\omega_{wT}}}} + R_{asymp} \tag{C.5}$$

because the original derivation of the expression of the Warburg impedance in mean-field [20] considered the particular solution of the differential equations in mean-field, also called the "forced solution". The general solution is the sum of this particular solution and the solution of the homogeneous equation ($\nabla^2 V_\omega = 0$). To take this into account, one needs to add a resistance in series with the forced solution ($R_{asymp.}$). This asymptotic resistance appears at very large frequencies in the experimental measurements (see Results).

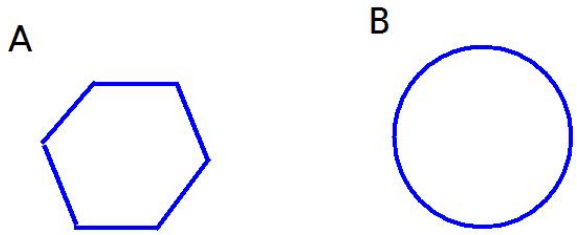

Figure D.1: Examples of how the curvature of isopotential surfaces determines the cutoff frequency of the impedance. A. Volume delimited by a plane (infinite curvature radius), resulting in a cutoff frequency near zero. B. Similar volume delimited by a border of constant curvature. In this case, the cutoff frequency is larger because it is inversely proportional to the curvature radius (Appendix D).

D Threshold frequency and surface curvature of the diffusive model in the general case

In this appendix, we give some details about the relation between the threshold frequency in the diffusive impedance (expression C.5) and the curvature at a given point of a surface S. In other words, we show how to apply the diffusive model to surfaces that are non-spherical.

The diffusive model of Appendix C can be applied to an arbitrary surface because we can build an approximately continuous surface $\mathcal{S}$ by the sum of portions of spherical surfaces centered on different points of $\mathcal{S}$, where the curvature corresponds to that of $\mathcal{S}$. Note that the smaller the intrinsic curvature of a surface, the smaller is the threshold frequency of that surface[1].

For example, if we have a surface $\mathcal{S}$ composed of two spherical portions ($\mathcal{S}_1$ and $\mathcal{S}_2$) of very different radius, the diffusive impedance diffusive as sensed by the surface is equal to the two impedances of each portion in parallel, because the current divides between both of them. It follows that $Z_S = Z_{S_1} \parallel Z_{S_2}$, with:

$$Z_S = \frac{A_w}{1+\sqrt{i\frac{\omega}{\omega_{wT}}}} \tag{D.1}$$

where

$$\begin{cases} A_w &= \frac{A_{w_1} A_{w_2}}{A_{w_1}+A_{w_2}} \\ \\ \frac{1}{\sqrt{\omega_{wT}}} &= \frac{\frac{A_{w_1}}{\sqrt{\omega_{s_2}}}+\frac{A_{w_2}}{\sqrt{\omega_{s_1}}}}{A_{w_1}+A_{w_2}} \end{cases} \tag{D.2}$$

If the surfaces $\mathcal{S}_1$ and $\mathcal{S}_2$ have the same impedance, then the impedance of $\mathcal{S}$ is twice smaller, but the threshold frequency remains the same. If each surface displays a similar Warburg amplitude but with different threshold frequencies, then we obtain

[1] A similar approach is classically used to model the electrical point effect [32].

$$\frac{1}{\sqrt{\omega_{wT}}} = \frac{1}{\sqrt{\omega_{s_1}}} + \frac{1}{\sqrt{\omega_{s_2}}}$$

It follows that if we approximate a given surface with a set of N spherical portions of same Warburg amplitude, the threshold frequency is given by:

$$\frac{1}{\sqrt{\omega_{wT}}} = \sum_{i=1}^{N} \frac{1}{\sqrt{\omega_{s_i}}} \tag{D.3}$$

Thus, the portions of surface with the smallest curvature will determine the threshold frequency of the ensemble, Consequently, it is possible to obtain a very small threshold frequency, even in a domain of a very small volume (Fig. D.1).

E Macroscopic impedance relative to ground

In this appendix, we consider the macroscopic impedance as sensed by the electrode injecting the current in the soma, via the dendrite, before reaching the ground, $Z_{in\ den}^{ground}$, and the impedance as seen by the current going to the ground independently of the dendrite, $Z_{out\ den}^{ground}$, for a ball-and-stick model in a resistive extracellular medium. Note that the impedance between the soma and the ground is given by $Z_{in\ den}^{ground} \parallel Z_{out\ den}^{ground}$.
We also consider that the cytoplasm is resistive, as well as the Debye layers surrounding the membrane. We will consider the experimental measurements of Section 3.2. Importantly, in the present experiments, the impedance between the cell and the ground should be calculated in an "open" configuration, because the current injected in the neuron flows to the ground without looping back to the neuron.
We numerically compared the impact of the two configurations, open and closed, at the basis of the dendrite (stick). In particular, the parameter $\kappa_\lambda = \kappa/\lambda$ is a good indicator to evaluate the differences between the two configurations.
For this purpose, we first assumed that the extracellular impedance $z_e^{(m)}$ has the same value at every point in the membrane in soma and dendrites. This hypothesis is reasonable if the neuron is physically smaller than the geometrical dimensions of the experimental preparation. Indeed, this parameter measures the impedance of the extracellular medium as sensed by the membrane, as defined by $z_e^{(m)}/dS$ which is the impedance between dS, a differential element of membrane, and the ground.

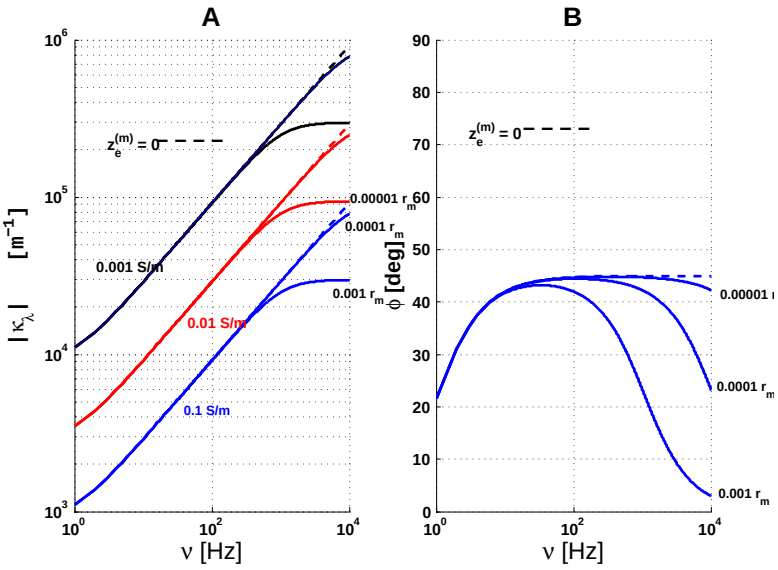

Figure E.1: Graph of $\frac{\kappa}{\lambda}$ as a function of frequency for the ball-and-stick model. Here, $\kappa = \sqrt{1 + i\omega\tau_m}$, the soma has a radius of 10 μm, while the length and diameter of the stick are respectively of 600 μm and 3 μm. In this example, the membrane time constant τ_m is of 30 ms, $c_m = 0.01\ F/m^2$ is the specific membrane capacitance, and $z_e^{(m)} = kr_m$ with $k = 0.001, 0.0001, 0.00001$. The dashed lines correspond to the open configuration, and continuous lines to the closed configuration. The electric conductivity of the cytoplasm σ_e^{nm} corresponds to the different colors, Blue: $\sigma_e^{nm} = 0.1 S/m$, Red: $\sigma_e^{nm} = 0.01 S/m$, Black: $\sigma_e^{nm} = 0.001 S/m$. Note that in the case $z_e^{(m)} = 0.00001 r_m$ is approximately equivalent to a supraconductive medium, for frequencies smaller than 10 kHz.

According to the generalized cable theory [22], for a resistive medium, we have:

$$\begin{cases} r_m &= \frac{e_m}{\sigma_e^{(mn)}} \\ z_e^{(m)} &= \frac{e_c}{\sigma_e^{(c)}} \end{cases} \tag{E.1}$$

where e_m and e_c are the thickness of the membrane and of Debye layers, respectively. $\sigma_e^{(mn)}$ and $\sigma_e^{(c)}$ are the mean electric conductivity of the membrane and of the extracellular medium (comprising Debye layers), respectively. Debye layers have a high density of ions, and thus have a different conductivity than the "bulk" of the medium. The ions around the membrane are distributed according to Boltzmann distribution, forming Debye layers, and the diffusive model must be taken into account in this case (Appendices C and D). The electric conductivity is much lower

in Debye layers compared to the other parts of the extracellular medium, which is considered homogeneous away of Debye layers. We assumed a thickness equivalent to that of Debye layers in the expression of $z_e^{(m)}$ (Eq. E.1).
However, in this appendix, we neglect the possible frequency dependence and model the impedance of Debye layers with a resistance, as if the threshold frequency was very large. The goal here is to determine, as simple as possible, the physical consequences of the magnitude of $|z_e^{(m)}|$ relative to r_m on the current division between the soma and the dendritic stick.
According to expressions E.1, we obtain:

$$z_e^{(m)} = \frac{e_c}{e_m} \frac{\sigma_e^{(mn)}}{\sigma_e^{(c)}} r_m \tag{E.2}$$

where $r_m = \tau_m / c_m = 100\tau_m$ (with $c_m = 0.01\ F/m^2$).
For a value of $\tau_m = 30\ ms$, $e_c = 0.1 e_m$ and $\sigma_e^{(mn)} = 10^{-2}\sigma_e^{(c)}$, we obtain $z_e^{(m)} = 0.003\ \Omega m^2$. This value gives the order of magnitude of the physical effects on the impedances $Z_{in\ den}^{ground}$ and $Z_{out\ den}^{ground}$. The value of the membrane time constant is that of the experiments presented here.
Next, from the evolution of the electric conductivity of the cytoplasm, we consider three different values: 0.1, 0.01 and 0.001 S/m (Fig. E.2) The first value approximately corresponds to that of ACSF for a temperature of 37 ^oC. The two other values are smaller, to simulate the fact that the cytoplasm is a heterogeneous medium (presence of organites), which creates a tortuosity, as well as electric polarization. These effects have been reported to diminish electric conductivity [27, 28].

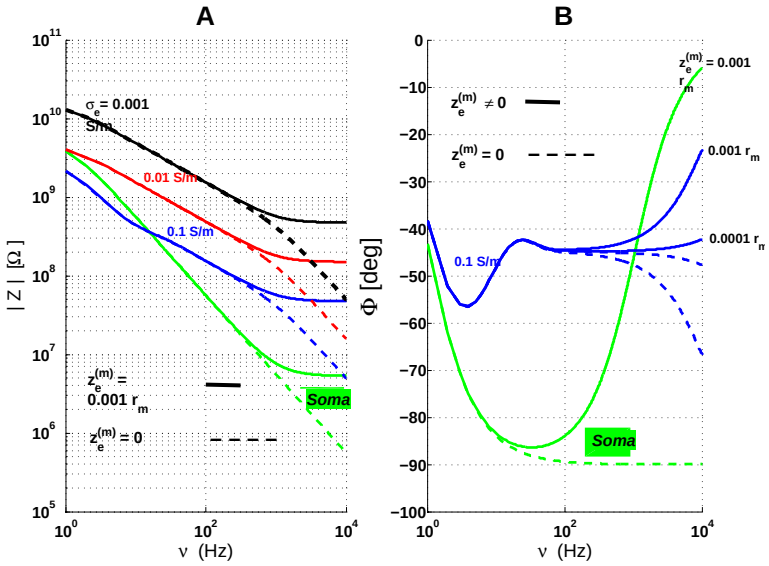

Figure E.2: Example of input impedance $Z^{ground}_{in\ den}$ and of soma impedance Z^{ground}_{soma}. Here, $z^{(m)}_e = kr_m$ and $k = 0.001, 0.0001$. The electric conductivity of the cytoplasm is $\sigma^{nm}_e = 0.1, 0.01, 0.001\ S/m$. The other parameters are the same as in Fig. D.1. The dotted lines correspond to the case $z^{(m)}_e = 0$, which is equivalent to neglect Debye layers; solid lines correspond to a resistive model, with Debye layers taken into account.

Figure E.2 shows examples of the input impedance in the following conditions. **1)** The open and closed configurations give very different results when $z^{(m)}_e > 0.01\tau_m\ \Omega m^2$, otherwise the differences are small for parameters κ_λ. Note that the case $z^{(m)}_e < 0.00001 r_m$ is as if Debye layers were inexistent for frequencies smaller than 10 kHz. **2)**. For $\sigma^{(nm)}_e = 0.1\ S/m$, $|Z^{ground}_{in\ den}| > |Z^{ground}_{soma}|$ if $\nu > 100\ Hz$, for $\sigma^{(nm)}_e = 0.01\ S/m$. This inequality holds up to about 1 Hz. For $\sigma^{(nm)}_e = 0.001\ S/m$, the modulus of the dendrite (stick) impedance is much larger than that of the soma.

F Apparent electric conductivity and permittivity

In this appendix, we define the apparent electric conductivity and permittivity. In general, we have the following linking relations between the diffusion $\vec{j}^f$,$\vec{E}$ and the fields $\vec{D}$,$\vec{E}$:

$$\begin{cases} \vec{j}^f(t) &= \int_{-\infty}^{t} f_\sigma(t-t')\ \vec{E}(t')\ dt' \\ \vec{D}(t) &= \int_{-\infty}^{t} g_\varepsilon(t-t')\ \vec{E}(t')\ dt' \end{cases} \tag{F.1}$$

This is obtained in the framework of a mean-field theory of Maxwell equations when the extracellular and intracellular media are linear and homogeneous [20, 35]. Note that the functions f_σ and g_ε are real functions which can model different physical phenomena, such as ionic diffusion, electric polarization, calorific (resistive) dissipation, etc. The integral expresses the fact that the free-charge current density and displacement current density at a given time t are not only determined by the electric field at time t but also by the whole history of its time variations. These functions are the inverse Fourier transform of electric conductivity and permittivity expressed in Fourier frequency space[2]. For example, for an ideal electric resistance, we have $f_\sigma(t) = \sigma_e \delta(t)$, for an ideal capacitance we have $g_\varepsilon(t) = \varepsilon_s \delta(t)$ (where σ_e are ε_s are constant in time). These two parameters are respectively the electric conductivity and permittivity. In these two ideal cases, the relations F.1 give the following equalities: $\vec{j}^f = \sigma_e \vec{E}$ and $D = \varepsilon_s \vec{E}$, where σ_e and ε_s are time independent. Note that these two ideal elements have no memory of the past (which is expressed by the Dirac deltas), and this is not generally the case of frequency-dependent electric conductivity and permittivity.
Consequently, we have in general, in Fourier frequency space:

$$\begin{cases} \vec{j}^f(\omega) &= \sigma(\omega)\ \vec{E}(\omega) \\ \vec{D}(\omega) &= \varepsilon(\omega)\ \vec{E}(\omega) \end{cases} \tag{F.2}$$

where $\sigma(\omega)$ and $\varepsilon(\omega)$ are respectively the Fourier transforms of $f_\sigma(t)$ and $g_\varepsilon(t)$. Because $f_\sigma(t)$ and $g_\varepsilon(t)$ are real functions, this implies in general $\sigma(-\omega) = \sigma^*(\omega)$ and $\varepsilon(-\omega) = \varepsilon^*(\omega)$. Here, the real parts are necessarily even functions and the imaginary parts are odd functions. The relations F.2 imply that the generalized current density is related to the electric field by:

$$\vec{j}^g(\omega) = \vec{j}^f(\omega) + \vec{j}^d(\omega) = [\sigma(\omega) + i\omega\varepsilon(\omega)]\ \vec{E}(\omega) = \gamma(\omega)\ \vec{E}(\omega) \tag{F.3}$$

where $\sigma = \sigma' + i\sigma''$ and $\varepsilon = \varepsilon' + i\varepsilon''$ are complex functions in general, while σ', σ'', ε', ε'' are real functions. We have the following particular cases: an ideal resistance is such that we have $\sigma(\omega) = \sigma_e$ (Ohm's law), an ideal capacitance corresponds to $\varepsilon(\omega) = \varepsilon$, so that σ and ε are real numbers and do not depend on frequency.
From these relations, we obtain:

$$\gamma = (\sigma' - \omega\varepsilon") + i\omega(\varepsilon' + \frac{\sigma''}{\omega}) = \sigma_{\mathcal{A}} + i\omega\varepsilon_{\mathcal{A}} \tag{F.4}$$

[2]Representing the electric parameters in Fourier frequency space is particularly efficient when the medium is linear because in this case the density of free-charge current and displacement current are proportional to $e^{i\omega t}$ if the electric field is also proportional to this term.

which defines the apparent electric conductivity $\sigma_{\mathcal{A}}$ and the apparent electric permittivity $\varepsilon_{\mathcal{A}}$. In general, the apparent electric permittivity can be viewed as a type of resistance which depends on frequency and allows to calculate the dissipated power at a given frequency. The ratio $\varepsilon_{\mathcal{A}}/\sigma_{\mathcal{A}}$ can be used to evaluate the relaxation time of the medium. Note that this definition corresponds to the electric parameters measured in previous studies [7, 34]. In these experimental studies, the measurements are characterized by parameters $\sigma_{\mathcal{A}}$ and $\varepsilon_{\mathcal{A}}$ because we interpret the experimental measurements in a very heterogeneous medium as if it was a non-ideal resistance (which depends on frequency) in parallel with a non-ideal capacitance (which also depends on frequency). A heterogeneous medium can be modeled as a homogeneous medium where the parameters depend on frequency with respect to macroscopic measurements. This is analogous to classical thermodynamics where pressure and temperature can be used to characterize a physical system.
Note that the apparent electric permittivity tends to infinity if the imaginary part of the electric conductivity does not tend to zero at null frequency. This is not the case for an ideal resistance because the imaginary part of its electric conductivity is zero. However, for a diffusive (planar) impedance (with zero curvature, see Appendix D) the imaginary part of electric conductivity is non-zero, since in this case $\gamma = k\sqrt{\omega}(1+i)$ where k is a constant.
By definition, the complex admittance Y between the two arms of a plane capacitor with a given medium in between, is given by $\frac{A}{d}\left[\sigma_{\mathcal{A}} + i\omega\varepsilon_{\mathcal{A}}\right]$. A is the arms area and d is the distance separating them. If we assume that these geometrical dimensions do not generate boundary effects, the electric field between the arms is of V/d where V is the voltage difference between the arms of the capacitor.

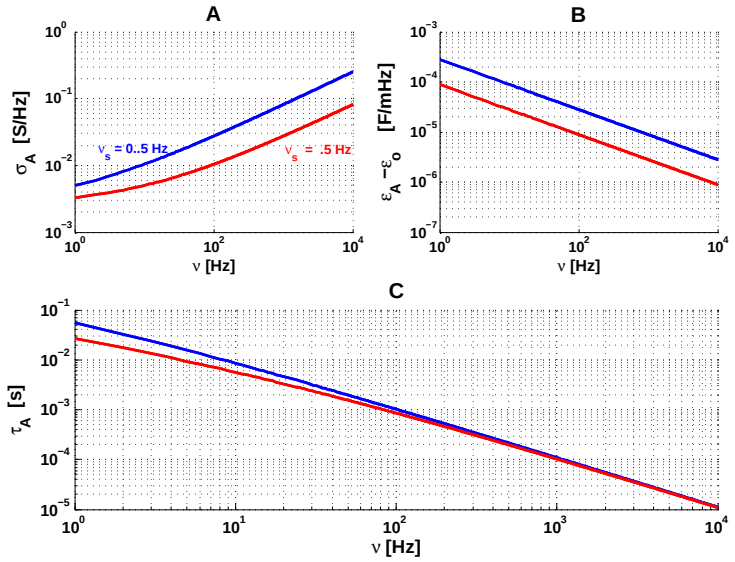

Figure F.1: Apparent conductivity and permittivity of a diffusive impedance. The red and blue curves correspond to $\nu_{wT} = .5\ Hz$ and black curves correspond to $\nu_{wT} = 40\ Hz$. We have $A_w = 16\ M\Omega$ and $A/d = 10\ \mu m$ for all curves,

For example, the measurement of the apparent parameters of a medium with a diffusive impedance gives the following equality:

$$Y = \frac{A}{d}\left[\sigma_{\mathcal{A}} + i\omega\varepsilon_{\mathcal{A}}\right] = \frac{1+\sqrt{i\frac{\omega}{\omega_{wT}}}}{A_w} \tag{F.5}$$

It follows that the frequency dependence of the parameters is given by the following expressions:

$$\begin{cases} k\sigma_{\mathcal{A}} &= 1+\sqrt{\frac{\omega}{2\omega_{wT}}} \\ k\varepsilon_{\mathcal{A}} &= \frac{1}{\sqrt{2\omega\omega_{wT}}} \\ \tau_{\mathcal{A}} &= \frac{\varepsilon_{\mathcal{A}}}{\sigma_{\mathcal{A}}} = \frac{1}{\omega+\sqrt{2\omega\omega_{wT}}} \end{cases} \tag{F.6}$$

where the constant k is equal to $\frac{AA_w}{d}$.
Thus, the apparent electric conductivity tends to k, the electric permittivity tends to infinite, and the dielectric relaxation time tends to infinity for $\omega \to 0$. We conclude

that if ionic diffusion is not negligible, then the linear approximation of its effect on the measured impedance is as if the dielectric relaxation time tends to infinity at null frequency (Fig. F.1).

G Ensemble of the measurements

In this appendix, we show the ensemble of experimental results obtained in the different preparations. Figures G.1 (non-arborized neurons in culture), G.3 (arborized neurons in culture) and G.5 (arborized neurons in brain slices) respectively show the impedance of Region 1-2 (between the intracellular and extracellular electrodes). The same preparations are respectively shown in Figs. G.2, G.4 and G.6 for the modulus of the impedance of Region 2-3 (between the extracellular electrode and the ground). The values of the experimental parameters for the different experimental preparations are shown respectively in Table G.1, G.3 and G.5, while the values of the corresponding models are shown in Table G.2, G.4 and G.6.

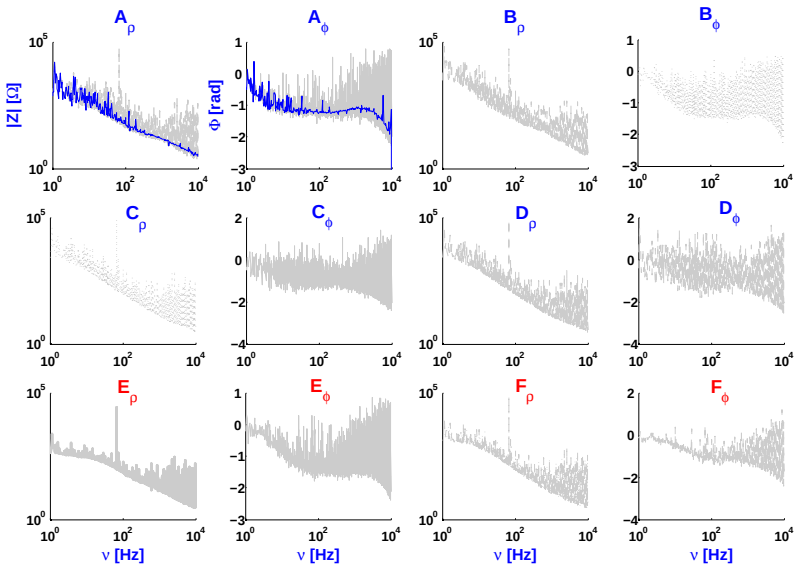

Figure G.1: Experimental measurement between intracellular and extracellular electrodes for 6 non-arborized neurons in culture. On the basis of the fits, two groups can be distinguished, one with τ_m around 30 ms and another group with 5-15 ms (Tables G.1 and G.2). The blue curves are cubic spline fits of the experimental data.

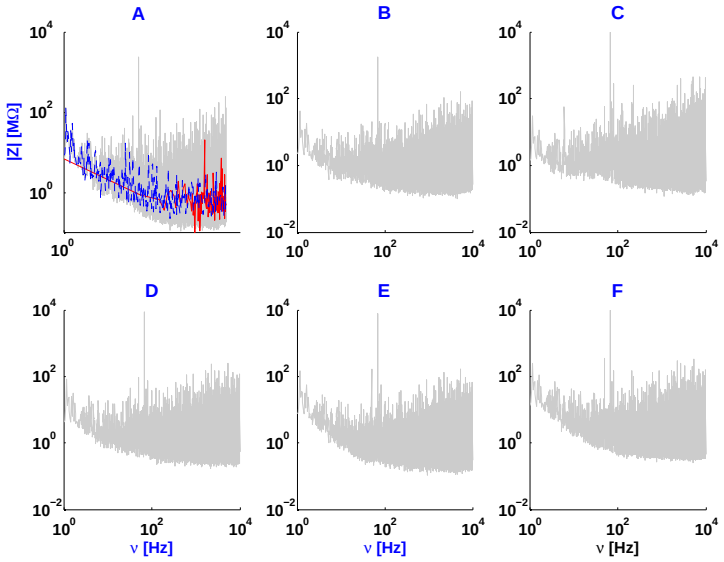

Figure G.2: Experimental measurements between extracellular and ground for 6 non-arborized neurons in primary cell culture, as shown in Tables G.1 and G.2. The blue curves are cubic spline fits to the logarithm of the experimental data, while the red curves are the direct cubic spline fits of the data.

	V_m (mean ± standard deviation) during white noise injection (mV)	σ of white noise current (pA)	Number of sweeps	Membrane resistance (MΩ) Membrane time constant (ms)
A : 2020021702	-68.9 ± 2.5	10	18	NaN NaN
B : 2020021801	-64.6 ± 6.4	5	13	2995 117
C : 2020021901	-62.3 ± 2.5	10	20	900 62
D : 2020021803	-57.7 ± 4.0	5	71	2090 105
E : 2020021802	-64.3 ± 1.6	10	14	558 16
F : 2020031503	-57.1 ± .9	5	25	1339 32

Table G.1: Individual experimental parameters for 6 non-arborized neurons in culture, shown in Fig. G.1. In the absence of measurements, a NaN is indicated.

	R_m $[M\Omega]$	τ_m $[ms]$	A_w $[M\Omega]$	ν_{wT} $[ms]$	R_{asymp} $[M\Omega]$	σ_d^{exp} $[M\Omega]$	σ_r^{exp} $[M\Omega]$
A	1000	30	625	0.1	4	3.4	142.9
B	3000	30	2000	0.2	4	16	225.0
C	3000	35	2000	0.05	6	3.5	210.0
D	3000	25	2000	0.05	3	3.8	215.0
E	3000	5	2000	0.7	2	2.9	58.3
F	1000	15	670	0,1	2	2.2	179.0

Table G.2: Parameters for the diffusive model for each non-arborized neuron in Table G.1. σ_r^{exp} and σ_d^{exp} are respectively the mean square error of resistive and diffusive models relative to the experimental measurements for each neuron .

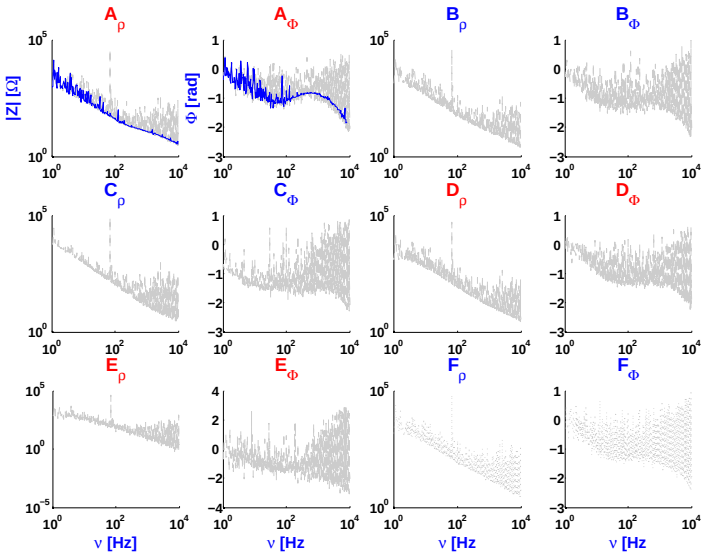

Figure G.3: Experimental measurements between intracellular and extracellular electrodes for 6 arborized neurons in primary cell culture (quasi-homogeneous medium). The blue curves are cubic spline fits of the experimental data.

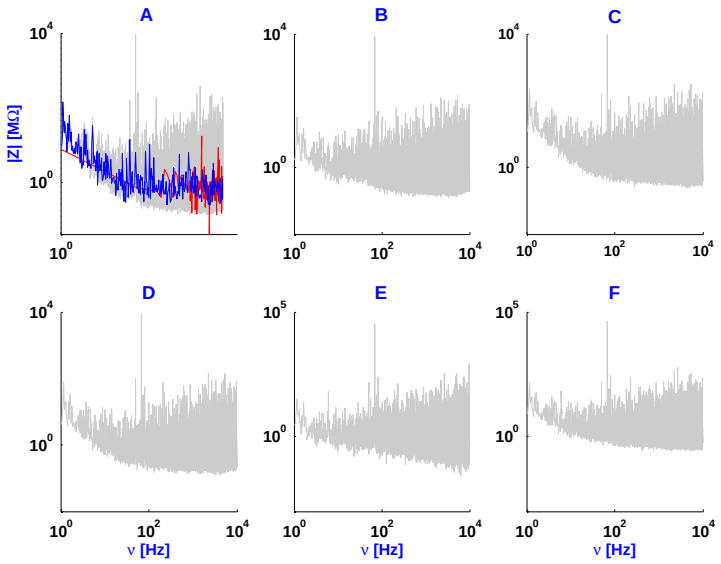

Figure G.4: Experimental measurements between extra and ground for 6 arborized neurons in culture, as shown in Tables G.3 and G.4. The blue curves are cubic spline fits to the logarithm of the experimental data, while the red curves are the direct cubic spline fits of the data.

	V_m (mean ± standard deviation) during white noise injection (mV)	σ of white noise current (pA)	Number of sweeps	Membrane resistance (MΩ) Membrane time constant (ms)
A : 2020021701	-66.0 ± 2.6	10	46	549 25
B : 2020021902	-68.1± 4.0	10	31	1820 67
C : 2020031501	-76.1 ± 4.4	5	28	4737 109
D : 2020031502	-67.5 ± 4.4	10	60	1347 31
E : 2020031602	-66.7 ± 2.1	10	3	793 22
F : 2020031603	-69.4 ± 2.7	5	26	2220 89

Table G.3: Individual experimental parameters for 6 arborized neurons in culture.

	R_m $[M\Omega]$	τ_m $[ms]$	A_w $[M\Omega]$	ν_{wT} $[ms]$	R_{asymp} $[M\Omega]$	σ_d^{exp} $[M\Omega]$	σ_r^{exp} $[M\Omega]$
A	3150	30	1050	0.02	2	2.0	223.0
B	2100	30	1260	0.01	0	2.5	129.0
C	1200	25	1000	0.03	0	2.0	97.0
D	1200	35	1200	0.02	3	3.8	101.0
E	1200	35	1200	0.03	3	3.1	108.0
F	1500	35	1500	0.02	0	4.1	131.0

Table G.4: Individual parameters obtained from fits for 6 arborized neurons in culture from Table G.3. σ_r^{exp} and σ_d^{exp} are respectively the mean square error of resistive and diffusive models with respect to the experimental data.

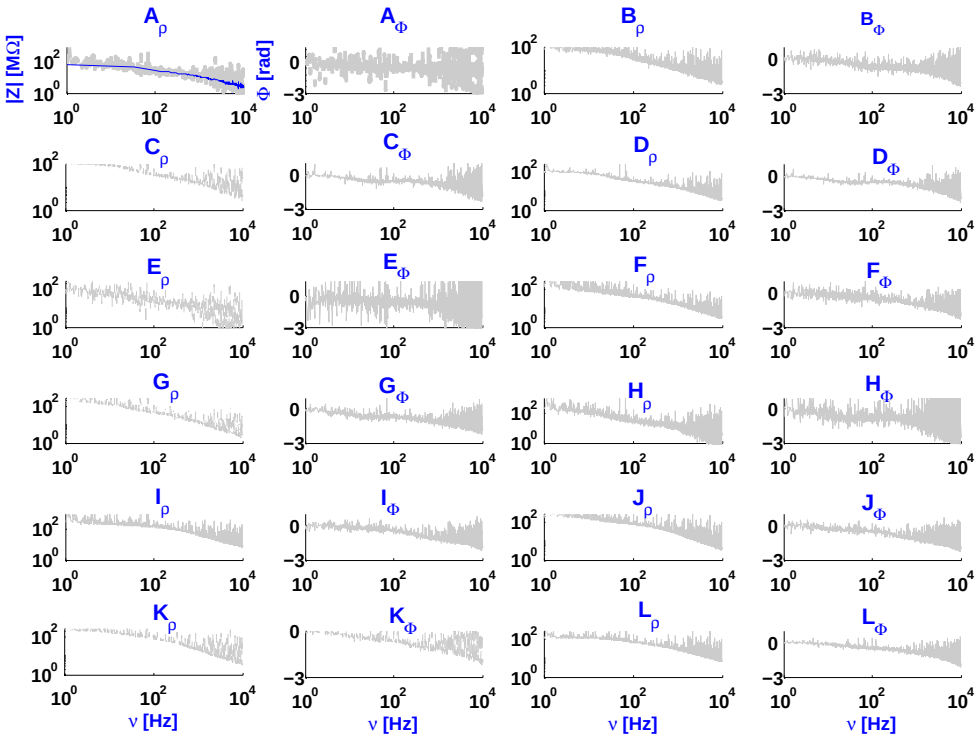

Figure G.5: Experimental measurements between intracellular and extracellular electrodes for 9 arborized neurons in brain slices, as shown in Tables G.5 and G.6. The blue curves are the cubic spline fits of the experimental data.

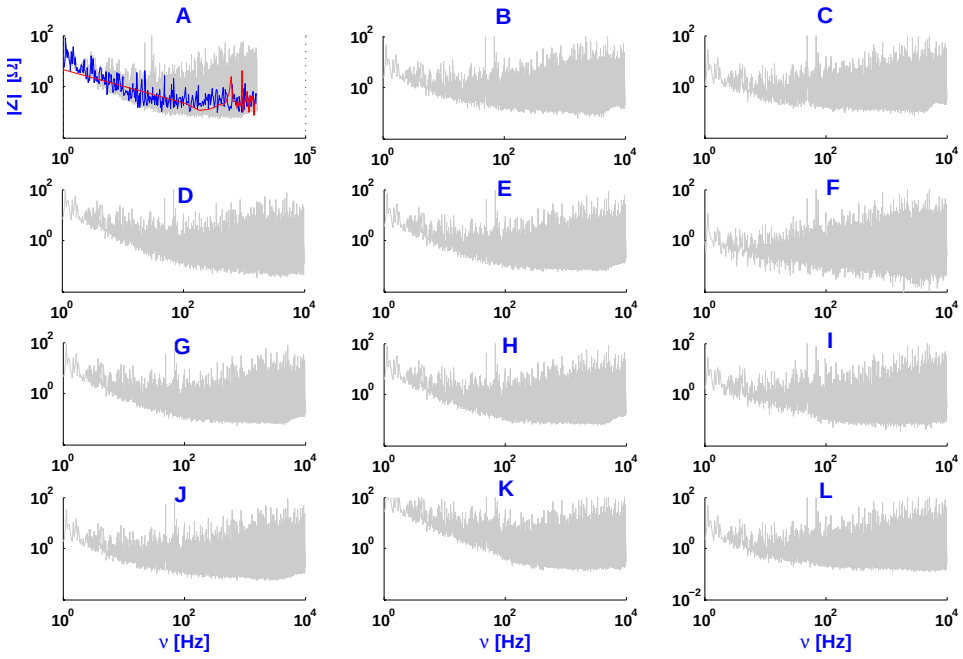

Figure G.6: Experimental measurements between extracellular and ground for arborized neurons in slices, as shown in Tables G.5 and G.6. The blue curves are cubic spline fits to the logarithm of the experimental data, and the red curves are the direct cubic spline fits of the data.

	V_m (mean ± standard deviation) during white noise injection (mV)	σ of white noise current (pA)	Number of sweeps	Membrane resistance (MΩ) Membrane time constant (ms)
A : 2018121204 (MSN)	-75.2 ± 1.1	20	1	67 6.0
B : 2018121205 (FS)	-74.8 ± 1.2	20	10	53 5.5
C : 2018122701 (FS)	-78.2± 1.3	20	15	124 5.6
D : 2019021202 (MSN)	-75.8 ± 1.3	20	6	83 4.2
E : 2019021203 (MSN)	-73.9 ± 1.7	20	59	85 4.0
F : 2019021302* (MSN)	-69.1 ± 1.8	20	13	64 7.7
G : 2019021304* (MSN)	-69.3 ± 1.7	20	10	128 9.5
H : 2019021401 (MSN)	-64.6 ± 1.4	10	5	124 8.4
I : 2019021801 (MSN)	-80.1 ± 2.7	10	31	92 2.8
J : 2019021802 (Cholinergic interneuron)	-73.3 ± 1.6	10	35	158 6.3
K : 2019021803* (MSN)	-67.1 ± 1.6	10	8	206 7.9
L : 2019021901 (MSN)	-76.8 ± 1.4	10	49	44 3.4

Table G.5: Individual experimental parameters for 9 arborized neurons in brain slices (MSN: medium-sized spiny neuron; FS: fast-spiking interneuron).

	$\bar{R}_m$ $[M\Omega]$	R_m $[M\Omega]$	τ_m $[ms]$	A_w^a $[M\Omega]$	ν_{wT}^a $[Hz]$	A_w^b $[M\Omega]$	ν_{wT}^b [Hz]	R_{asymp} $[M\Omega]$	σ_d^{exp} $[M\Omega]$	σ_r^{exp} $[M\Omega]$
A	120	48	5	48	5	24	40	1	2.1	6.0
B	120	50	5	50	5	24	40	4	2.3	6.6
C	140	47	5	47	5	40	60	4	2.3	5.2
D	140	48	5	48	1	40	60	2	2.4	5.1
E	140	48	2.5	48	1	40	60	1	2.0	6.0
F	140	48	5	48	1	40	60	4	5.5	11.0
G	256	90	20	90	1	75	40	1	6.3.	9.5
H	256	90	20	90	0.1	75	10	1	3.0	10.1
I	426	150	1	150	1	125	20	1	28.1	72.0
J	320.5	90	10	90	20	125	60	.5	6.1	26.3
K	320.5	90	10	90	20	75	60	.5	6.1	26.3
L	320.5	48	1	48	45	40	80	3	6.3	15.3

Table G.6: Individual parameters obtained from the fits for arborized neurons in brain slices from Table G.5. The total resistance for $\nu = 0$ is equal to $\bar{R}_m = R_m + A_w^a + A_w^b + R_{asymp}$. σ_r^{exp} and σ_d^{exp} are the mean square errors of the resistive and diffusive models relative to experimental data, respectively.

The extracellular-to-ground measurements are similar in all preparations and exhibit a similar frequency dependence. All fits show that the impedance modulus of the extracellular medium is of the order of that of ACSF.
However, this is not the case for the intracellular-to-extracellular measurements in the different preparations. For all cells and for all preparations, the diffusive model fits better the experimental data.
Finally, for the different preparations, the experimental measurements (membrane resistance and membrane time constant) shown in Table G.1 are different from that displayed in Table G.2. This difference shows that the evaluation of the membrane time constant using a current pulse leads to different membrane time constants as those evaluated from direct fitting of the impedance. This aspect is examined in more detail in the following (Appendix H).

H Voltage between two points for a square current pulse

In this appendix, we calculate the voltage between two points when the injected current is a square pulse.
We model a pulse of current as follows:

$$I^g = h\left[H(t) - H(t-\Delta)\right] \ , \tag{H.1}$$

where $\Delta > 0$ is duration of the current pulse, and H is the Heaviside function.
The most general linear relation between current and voltage is given by the following expression:

$$V(t) = \int_{-\infty}^{+\infty} Z(t-t')\ I^g(t')\ dt' = \int_{-\infty}^{+\infty} Z(t')\ I^g(t-t')\ dt' \tag{H.2}$$

It follows that the derivative of the voltage is given by:

$$\frac{dV}{dt} = h\left[\ \int_{0^-}^{+\infty} Z(t')\ \delta(t-t')\ dt' - \int_{\Delta^-}^{+\infty} Z(t')\ \delta(t-\Delta-t')\ dt'\ \right]. \tag{H.3}$$

with $\frac{dI}{dt} = h[\delta(t) - \delta(t-\Delta)]$.
Thus, we obtain the following equality:

$$\frac{dV}{dt} = h[Z(t) - Z(t-\Delta)] \tag{H.4}$$

According to the complex Fourier transform,

$$\begin{cases} Z(t) &= PP\ [\ \frac{1}{2\pi} \int\limits_{-\infty}^{+\infty} Z(\omega)\ e^{i\omega t} d\omega\ ] \quad (a) \\ \\ V(t) &= PP\ [\ \frac{1}{2\pi} \int\limits_{-\infty}^{+\infty} V(\omega)\ e^{i\omega t} d\omega\ ] \quad (b) \end{cases} \tag{H.5}$$

where PP means the principal part of the integral.
In a diffusive medium, we have:

$$Z(\omega) = \frac{R_m}{1+i\omega\tau_m} + \frac{A_w}{1+\sqrt{i\omega\tau_{wT}}} + R_{asymp} \tag{H.6}$$

where $\tau_{wT} = 1/\omega_{wT}$. We calculate $\frac{dV}{dt}$ from Equations H.4 and H.5.
Applying Eq. H.5(a) on the right-hand part of Expression H.6 gives [37]).

$$\frac{dV}{dt} = hH(t)F(t) - hH(t-\Delta)F(t-\Delta) \tag{H.7}$$

where

$$F(t) = \frac{R_m}{\tau_m}\ e^{-\frac{t}{\tau_m}} + \frac{A_w}{\tau_{wT}}\left[\frac{1}{\sqrt{\pi}\sqrt{\frac{t}{\tau_{wT}}}} - e^{\frac{t}{\tau_{wT}}}\ erfc\left(\sqrt{\frac{t}{\tau_{wT}}}\right)\right] + R_{asymp}\delta(t) \quad \text{(H.8)}$$

The function $e^x \cdot erfc(\sqrt{x})$ for $x \geq 0$ is a real and positive monotonously decreasing function which tends to zero at infinite. At $x = 0$, it is equal to 1.
Because the experimental measurements shown here indicates that $\tau_m << \tau_{wT}$, we develop F(t) in series around zero to evaluate this function when $t < \tau_{wT}$. We obtain

$$\begin{cases} e^{t/\tau_{wT}} & = & 1 + \frac{t}{\tau_{wT}} + 0(2) \\ \\ erfc(\sqrt{t/\tau_{wT}}) & = & 1 - \frac{1}{\sqrt{\pi}}\left[2(\frac{t}{\tau_{wT}})^{1/2} - \frac{2}{3}(\frac{t}{\tau_{wT}})^{3/2} + 0(5/2)\right] \end{cases} \quad \text{(H.9)}$$

We then write the following equalities:

$$F(t) = \frac{R_m}{\tau_m}e^{-\frac{t}{\tau_m}} - \frac{A_w}{\tau_{wT}}\left[1 + \frac{t}{\tau_{wT}}\right] + \frac{A_w}{\tau_{wT}\sqrt{\pi}}\left[\frac{t^{-1/2}}{\tau_{wT}^{-1/2}} + 2\frac{t^{+1/2}}{\tau_{wT}^{+1/2}}\right] + R_{asymp}\delta(t) + 0(3/2) \quad \text{(H.10)}$$

and

$$G(t) = \int_{0^-}^{t} F(t')dt' = R_m(1 - e^{-\frac{t}{\tau_m}}) - A_w\frac{t}{\tau_{wT}} + \frac{2A_w}{\sqrt{\pi}}\frac{t^{1/2}}{\tau_{wT}^{1/2}} + R_{asymp} + 0(3/2) \quad \text{(H.11)}$$

The voltage for $V(0^-) = 0$ at $t = 0$ and $t \geq \Delta$ is given by (H.7)

$$V(t) = \overbrace{h\int_0^{\Delta} F(t')dt'}^{A} + \overbrace{h\int_{\Delta}^{t} F(t')dt'}^{B} - \overbrace{h\int_{\Delta}^{t} F(t'-\Delta)dt'}^{C} \quad \text{(H.12)}$$

which gives

$$\begin{cases} A(\Delta;0) & = & h[G(\Delta) - G(0)] \\ \\ B(t;\Delta) & = & h\ [G(t) - G(\Delta)] \\ \\ C(t;\Delta) & = & h\ [G(t-\Delta) - G(0)] \end{cases} \quad \text{(H.13)}$$

Thus, we have

$$\begin{cases} A(\Delta;0) &= hR_m\left[1-e^{-\frac{\Delta}{\tau_m}}\right]+hA_w\underbrace{\left[\frac{2}{\sqrt{\pi}}\frac{\Delta^{1/2}}{\tau_{wT}^{1/2}}-\frac{\Delta}{\tau_{wT}}\right]}_{>0} \\ B(t;\Delta) &= hR_m e^{-\frac{\Delta}{\tau_m}}\left[1-e^{-\frac{t-\Delta}{\tau_m}}\right]+hA_w\underbrace{\left[\frac{2}{\sqrt{\pi}}\frac{t^{1/2}-\Delta^{1/2}}{\tau_{wT}^{1/2}}-\frac{t-\Delta}{\tau_{wT}}\right]}_{>0} \\ C(t;\Delta) &= hR_m\left[1-e^{-\frac{t-\Delta}{\tau_m}}\right]+hA_w\underbrace{\left[\frac{2}{\sqrt{\pi}}\frac{(t-\Delta)^{1/2}}{\tau_{wT}^{1/2}}-\frac{t-\Delta}{\tau_{wT}}\right]}_{>0} \end{cases} \quad \text{(H.14)}$$

$A(\Delta)$ corresponds to the voltage reached at time Δ (Δ is the duration of the current pulse). $A(\Delta)$ depends on A_w. If $A_w = 0$, the voltage is equal to that of a resistive model. In the case of a diffusive model $A_w \neq 0$ is positive because $\frac{\Delta}{\tau_{wT}} < \frac{t}{\tau_{wT}} < 1$. Consequently, the voltage as a function of time is given by:

$$V(t) = \overbrace{hR_m[1-e^{-\frac{\Delta}{\tau_m}}]e^{-\frac{t-\Delta}{\tau_m}}}^{resistive\ model} + hA_w\left[-\frac{\Delta}{\tau_{wT}}+\frac{2}{\sqrt{\pi}}\left(\frac{t^{1/2}}{\tau_{wT}^{1/2}}-\frac{(t-\Delta)^{1/2}}{\tau_{wT}^{1/2}}\right)\right]+0(3/2) \quad \text{(H.15)}$$

when $t > \Delta$ and $t < \tau_{wT}$.
Finally, the last expression is equivalent to the second-order approximation in $\sqrt{t}$ of the expression

$$V(t) = \overbrace{hR_m[1-e^{-\frac{\Delta}{\tau_m}}]e^{-\frac{t-\Delta}{\tau_m}}}^{resistive\ model} - hAw[1-e^{-\frac{\Delta}{\tau_{wT}}}]e^{-\frac{t-\Delta}{\tau_{wT}}}+\frac{2}{\sqrt{\pi}}hA_w\left[1-e^{\left(\sqrt{\frac{t-\Delta}{\tau_{wT}}}-\sqrt{\frac{t}{\tau_{wT}}}\right)}\right]e^{-\sqrt{\frac{t-\Delta}{\tau_{wT}}}}+0(3/2) \quad \text{(H.16)}$$

when $t > \Delta$ and $t < \tau_{wT}$. We can also develop the third term of expression H.16 as a series of exponentials linear in t (using Newton binomial) with a combination of exponentials with different relaxation times.

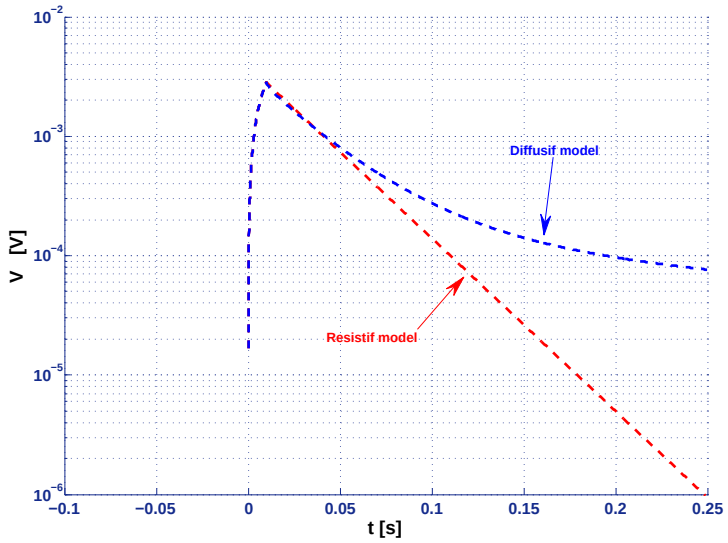

Figure H.1: Voltage relative to rest as a function of time during the injection of a current pulse of 10 pA and 10 ms duration. The membrane time constant was $\tau_m = 30\ ms$ and the impedance of the extracellular medium + membrane is of 1000 $M\Omega$ at null frequency. The red curve shows the prediction of the resistive model, while the blue curve shows the resistive model (with a threshold frequency of $\nu_{wT} = 0.5\ Hz$ and $A_w = R_m$).

Consequently, the method of current pulse injection and the linearization method give a different slope in a semi-log graph, according to the type of model. For a resistive model, the slope is $-1/\tau_m$, and this allows to directly estimate the membrane time constant, as classically performed. However, for a diffusive model, the slope is slightly variable and smaller than the resistive model. It depends on τ_m, ν_{wT} and on the ratio R_m/A_w. For $t > \Delta$, one part of the voltage, V_a ($V = V_a + V_b$), attenuates according to the resistive model, while the other part, V_b, attenuates slower and depends on ν_{wT}. This explains why the membrane time constant seems larger with the pulse or linearization method, compared to the fitting of experimental measurements (Appendix G). The divergence originates from the pulse or linearization methods according to a resistive model.

References

[1] Buzsáki, G., Anastassiou, C., and Koch, C. 2012. *The origin of extracellular fields and currents: EEG, ECoG, LFP and spikes.* Nature Reviews Neurosci. *13*, 407-420.

[2] Makarova, J., Gomez-Gala, M., and Herreras, O. (2008). *Variations in tissue resistivity and in the extension of activated neuron domains shape the voltage signal during spreading depression in the CA1 in vivo.* European Journal of Neuroscience *27*: 444-456.

[3] Rall, W.,G.M. Shepherd.1968. *Theoretical Reconstruction of Field Potentials and Dendrodendritic Synaptic Interactions in Olfactory Bulb* J Neurophysiol. Nov;31(6):884-915. doi: 10.1152/jn.1968.31.6.884.

[4] Ranck, J..1963. *Analysis of specific impedance of rabbit cerebral cortex.* Exp. Neurol. *7*, 144-152.

[5] Logothetis, N.K.,C. Kayser, and A. Oeltermann. 2007. *In vivo measurement of cortical impedance spectrum in monkeys: implications for signal propagation.* Neuron *55*: 809-823.

[6] Miceli, S., T.V. Ness, G.T. Einevoll, and D. Schubert . 2017. *Impedance Spectrum in Cortical Tissue: Implications for Propagation of LFP Signals on the Microscopic Level.* eNeuro,Jan-Feb; 4(1).

[7] Gabriel, S., R.W. Lau, and C. Gabriel.1996. *The dielectric properties of biological tissues: II. Measurements in the frequency range 10 Hz to 20 GHz.* Phys. Med. Biol., 41, 2251 .

[8] Wagner, T., U. Eden, J. Rushmore, C.J. Russo, L, Dipietro, F. Fregni, S. Simon, S. Rotman, N.B. Pitskel, C. Ramos-Estebanez, A. Pascual-Leone, A.J. Grodzinsky, M. Zahn, and A. Valero-Cabre. 2014. *Impact of brain tissue filtering on neurostimulation fields: a modeling study.* Neuroimage, Jan 15; 85(0 3): 1048-1057.

[9] Gomes, JM, C. Bédard, S. Valtcheva, MJ. Nelson, V. Khokhlova, P. Pouget, L. Venance, T. Bal and A. Destexhe. 2016. *Intracellular impedance measurements reveal non-ohmic properties of the extracellular medium around neurons. Biophys. J.* **110**: 234-246.

[10] Bédard, C., H. Kröger, A. Destexhe. 2004. *Modeling extracellular field potentials and the frequency-filtering properties of extracellular space.* Biophys. J. 64:1829-1842.

[11] Bedard, C., H. Kroger and A. Destexhe. 2006. *Model of low-pass filtering of local field potentials in brain tissue* Phys. Rev. E 73:051911.

[12] Bédard, C., Destexhe, A.. 2009. *Macroscopic models of local field potentials and the apparent 1/f noise in brain activity.* Biophys. J. 96(7):2589-4608.

[13] Bedard, C., S. Rodrigues, N. Roy, D. Contreras, A. Destexhe. 2010. *Evidence for frequency-dependent extracellular impedance from the transfer function between extracellular and intracellular potentials: intracellular-LFP transfer function* J. Comput. Neurosci. Dec;29(3):389-403.

[14] Dehghani, N., C. Bedard, S.S. Cash, E. Halgren, A. Destexhe . 2010. *Comparative power spectral analysis of simultaneous elecroencephalographic and magnetoencephalographic recordings in humans suggests non-resistive extracellular media.* J. Comput. neurosci. 29 (3): 405-421.

[15] Bedard, C., JM. Gomes, T. Bal, A. Destexhe . 2017.*A framework to reconcile frequency scaling measurements, from intracellular recordings, local-field potentials, up to EEG and MEG signals.* Journal of Integrative Neuroscience 16 (1): 3-18.

[16] Barbour, B. 2017. *Analysis of Claims that the Brain Extracellular Impedance Is High and Non-resistive*, Biophys. J. Volume 113, Issue 7, 1636-1638.

[17] Bedard, C. and Destexhe, A. 2017. *Is the extracellular impedance high and non-resistive in cerebral cortex ?*, Biophys. J. Volume 113, Issue 7, 1639-1642.

[18] Nelson, MJ.,P. Pouget, E. A. Nilsen,C. D. Patten, and J. D. Schall. 2008. *Review of Signal Distorsion through Metal Microelectrode Recordinf Circuits and Filters*, J Neurosci Methods, Mar 30; 169(1): 141-157.

[19] Nelson, MJ, S. Valtcheva, L. Venance. 2017. *Magnitude and behavior of cross-talk effects in multichannel electrophysiology experiments.* J Neurophysiol. 118: 574-594.

[20] Bédard, C., A Destexhe . 2011. *Generalized theory for current-source-density analysis in brain tissue*, Phys. Rev. E 84 (4):041909.

[21] Le Bellac, M., Lévy-Leblond J.M. . 1973. *Galilean electromagnetism.* Nuovo Cim B 14, 217-234 .

[22] Bédard, C. and Destexhe, A. . 2013. *Generalized cable theory for neurons in complex and heterogeneous media.* Physical Review E 88:022709.

[23] Rall, W.. 1995. *The theoretical foundations of dendritic function.*MIT Press, Cambridge, MA.

[24] Tuckwell, H.C.. 1988. *Introduction to Theoretical Neurobiology: Linear Cable Theory and Dendritic Structure.* Cambridge University Press, Cambdridge, UK.

[25] Bartels, R.H., J.C. Beatty, B.A. Barsky. 1987. *An Introduction to Splines for uses in Computer Graphics and Geometric Modeling* . Ed. Morgan Kaufman Publishers, Inc, Los Altos, California, 485 p.

[26] Johnston, D. and Wu S.M. 1995. *Foundations of Cellular Neurophysiology* , Ed. MIT Press.

[27] Maxwell, J.C. . 1873 *A Treatise on Electricity and Magnetism.* Clarendon Press, Oxford. Vol. 1

[28] Priou, A. . 1992. *Dielectric properties of heterogeneous materiels* . Progress in Electromagnetics Research, Elsevier, New York.

[29] Vasiliev, A. M.. 1984. *Introduction To Statistical Physics*, Ed. Mir.

[30] Nicholson, C. . 2005. *Factors governing diffusing molecular signals in brain extracellular space*. J. Neural Transm. *112*, 29-44 .

[31] Destexhe, A. and Bédard C.. 2013. *Local Field Potential*. Scholarpedia, http://www.scholarpedia.org/article/Local_field_potential

[32] Kalachnikov, S.. 1980. *Electricity*, Ed. Mir.

[33] Goldstein, H., C.P. Poole, J.L. Safko. 2001. *Classical Mechanics (3rd Edition)* . Ed. Addison Wesley, 647 p.

[34] Foster, K. R., H.P. Schwan . 1989. *Dielectric properties of tissues and biological materials: A critical review*. Critical Reviews in Biomedical Engineering 17(1):25-104.

[35] Bedard, C., Destexhe A. .2014. *Mean-field formulation of Maxwell equations to model electrically inhomogeneous and isotropic media Equations to Model Electrically*. Journal of Electromagnetic Analysis and Applications 6 (10), 296.

[36] Bedard, C., Destexhe A. .2014. *Generalized cable formalism to calculate the magnetic field of single neurons and neuronal populations*. Physical Review E 90 (4):042723.

[37] Oberhettinger, F. and L. Badii. 1973. *Tables of Laplace Transforms*. Springer-Verlag Berlin Heidelberg, New York.

[38] Rall, W. .1995. *The Theoretical Foundation of Dendritic Function*. Segev, I., J. Rinzel and G.M. Shepherd, ed. MIT Press, Cambridge MA.

[39] Hines, M.L., and N.T. Carnevale. 1997. The NEURON simulation environment. Neural Computation 9: 1179-1209.

[40] Nelson, MJ., C. Bosch, L. Venance, and P. Pouget . 2013. *Microscale Inhomogeneity of Brain Tissue Distorts Electrical Signal Propagation*. The Journal of Neuroscience,33(7):2821-2827.

[41] Hrabetova S, Cognet L, Rusakov DA, Nagerl UV. 2018. Unveiling the extracellular space of the brain: from super-resolved microstructure to in vivo function. J Neurosci. 38: 9355-9363.

[42] Herreras, O. 2016, *Local Field Potentials : Myths and Misunderstandings*. Front. Neural Circuits, 10 : 101. https://doi.org/10.3389/fncir.2016.00101